EFFECT OF CO CONTENT ON STRUCTURAL & MAGNETIC PROPERTIES OF MANGANESE COPPER FERRITES SYNTHESIZED BY SOL GEL AUTO COMBUSTION METHOD

P.V. Gaikwad[1], P.D. Kamble [2], M.R. Kadam[3], S.D. Zimur[4]
[1,2,3,4]PG, Department of Chemistry, Balasaheb Desai College, Affiliated to Shivaji University, Kolhapur, Patan, MS, India

Abstract
Single phase ferrites of Manganese, Cobalt and Copper i.e. $Mn_{0.5-X}Co_XCu_{0.5}Fe_2O_4$ ($0.0 \geq X \leq 0.5$) are prepared by using sol-gel auto combustion method. X-ray diffraction studies reveal that ferrites are polycrystalline with spinel structure. Lattice parameters of the same vary in the range of 8.33–8.39 A^0 with composition (X) obeying Vegard's rule. Micro grain size and compositional features of all samples were studied by scanning electron microscopy and energy dispersive X-ray analysis techniques respectively. Thermal analysis technique was used to decide sintering temperature of the ferrites. Electrical properties of the compounds exhibit semiconducting behavior. The magnetic properties are studied by using M-H hysteresis curves. The maximum value of the magnetization (41emu/g) was observed for $Co_{0.5}Cu_{0.5}Fe_2O_4$.

Keywords: A. Sol-gel processes, B. Electron Microscopy, C. X-ray diffraction, D. Magnetic Properties, E. Semiconductor.

1. INTRODUCTION

Spinel ferrites are iron based semiconducting oxides with technologically interesting magnetic properties, making them a famous group in magnetic materials, because of their potential applications in various interdisciplinary areas [1]. The synthesis of spinel type nano-structured magnetic materials with the general formula $M^{2+}(Fe^{3+})_2O_4$ (where M^{2+}=Mn^{2+}, Co^{2+}, Ni^{2+}, Cu^{2+}, Zn^{2+}, etc.) has become an important part of modern ceramic research, due to their unique physical and chemical properties than that of their bulk counterparts [2]. Among various spinel ferrites, cobalt ferrite ($CoFe_2O_4$) is especially interesting, because of their high cubic magneto crystalline anisotropy, excellent chemical stability, low toxicity, readily accessibility, high coercivity, moderate magnetization (M_s) and inexpensiveness, which make it a promising material as catalysts support [3–5]. Copper ferrite ($CuFe_2O_4$) has mostly an inverse spinel structure [6]. The cation distribution in the copper ferrite can be presented by the stoichiometric relation: $[Cu^{2+}_{d} Fe^{3+}_{1-d}]_A [Cu^{2+}_{1-d} + Fe^{3+}_{1+d}]_B O_4$. The parameter of inversion, d is equal to 0 for inverted spinels and 1 when the spinel is normal. Cu^{2+} cations migrate from octahedral (B sub lattice) to tetrahedral places (A sub lattice) [7]. Various research groups have studied the effect of doping with different cations to enhance physical properties of spinel ferrites [8]. In electronic structure studies of Cu^{2+} doped cobalt ferrite, they observed that Cu^{2+} ions occupy octahedral site [9].

Recently, considerable efforts have been made on the surface modification and the preparation of different types of metal oxides. Various methods are available for the synthesis of metal oxides, such as co-precipitation [10], sol–gel [11,12], spray pyrolysis [13], hydrothermal [14,15], microwave refluxing [16], citrate–gel [17], etc. The selection of appropriate synthetic procedure often depends on the desired properties and final applications. Among these synthesis techniques, sol–gel auto combustion

method have several advantages over others for preparation of metal oxides as the process begins with a relatively homogeneous mixture and involves low temperature conditions resulting in a uniform ultrafine porous powders [18, 19]. The aim of present work is to investigate structural, electrical and magnetic properties of $Mn_{0.5-x}Co_xCu_{0.5}Fe_2O_4$ ($0.0 \geq X \leq 0.5$) system. Structural and morphological properties are investigated by X-ray diffraction (XRD) and SEM. Elemental analysis was carried out by energy dispersive X-ray spectroscopy and electrical resistivity measurements by using two probe methods. Magnetic properties were studied by using hysteresis loop tracer.

2. EXPERIMENTAL TECHNIQUE

2.1 Synthetic Technique

Polycrystalline $Mn_{0.5-x}Co_xCu_{0.5}Fe_2O_4$ powders ($0.0 \geq X \leq 0.5$) were synthesized by sol–gel auto-combustion method with analytical grade Manganese nitrate [$Mn(NO_3)_2 \cdot 4H_2O$], Cobalt nitrate [$Co(NO_3)_3.6H_2O$], Copper nitrate [$Cu(NO_3)_3.3H_2O$], Iron nitrate [$Fe(NO_3)_3 \cdot 9H_2O$] and Urea [NH_2CONH_2]. Metal nitrates and urea were dissolved in minimum quantity of deionized water with stoichiometric proportions and solutions were mixed. The pH of the solution was maintained to 9.0–9.5 using ammonia solution. The solution was transformed into dry gel on heating at 373 K. On further heating the dried gel burnt in a self propagating combustion manner till whole quantity of gel get completely converted to a floppy loose powder. Later burnt precursor powder was sintered at 1273K for 5 hours. The used synthesis process i.e., auto combustion has various advantages such as simple, inexpensive, quick synthesis and does not required any vacuum process or sophisticated instrumentation.

2.2 Characterization

A computerized X-ray powder diffractometer (Siemens D-500 diffractometer) with Cu-Kα radiation (λ=1.5406 Å) was used to identify the crystalline nature of the samples and to calculate lattice parameter and crystallite size. The lattice parameters were calculated for the cubic phase using following relation.

$$\frac{1}{d^2} = \frac{h^2}{a^2} + \frac{k^2}{b^2} + \frac{l^2}{c^2} \ldots\ldots\ldots\ldots [1]$$

Where a, b and c are lattice parameters, (hkl) is the Miller indices and d is the interplanar distance.

From the X-ray diffraction peaks, crystallite size was estimated using Debye Scherer's formula [20]

$$t = \frac{0.9\,\lambda}{\beta \cos\theta} \ldots\ldots\ldots\ldots [2]$$

Where, symbols have their usual meaning.

The X-ray density (dx) was calculated by using the relation,

$$dx = \frac{8M}{Na^3} \ldots\ldots\ldots [3]$$

Where N= Avogadro's number (6.023×10^{23} atom/mol), M= molecular weight and a = lattice constant.

The percentage porosity of sample was calculated using the formula

$$P(\%) = \left(\frac{d_a - d_x}{d_a}\right) x\ 100 \ldots\ldots\ldots [4]$$

Where d_a = actual density and d_x = theoretical density.

Formation temperature of samples was checked by taking TGA/DTA curves on the SDT Q600 V20.9 instrument by heating the powders at a rate of 10°C/min from room temperature to 1000°C in an air atmosphere. Scanning electron microscope (SEM) was used to study the morphology of the powders. The grain size of all the samples was calculated by Cottrell's method. An energy dispersive X-ray spectroscopy analyzer equipped with SEM was used for the compositional analysis.

The electrical resistivity measurements in the temperature range from 323 to 773 K were taken by two probe method. The electrical contacts were established by pasting silver paste on both surfaces of the pellet. The graphs of the logρ vs. 1000/T was plotted for all the samples under investigation and their energy of activation values (E_a) were calculated by using the equation:

$$E_a = 1.983\ x\ 10^{-4}\left(\frac{\log\rho}{\frac{1}{T}}\right) \text{ev} \ldots\ldots\ldots [5]$$

Where, symbols have their usual meaning.

A computerized high field hysteresis loop tracer was used to measure magnetic properties at room temperature for all compositions. The magnetic moment per formula unit in Bohr magnetron (μ_B) was calculated by using the relation [21].

$$\mu_B = \frac{MW\ x\ M_s}{5585} \ldots\ldots\ldots [6]$$

Where, MW=molecular weight of composition (in grams); M_S = saturation magnetization (in emu/gm).

3. RESULTS AND DISCUSSION

3.1. X-ray diffraction studies

The structure and phase purity of the product were confirmed by analyzing the observed powder X-ray diffraction patterns. Fig. 1 depicts the observed powder XRD patterns of the prepared $Mn_{0.5-X}Co_XCu_{0.5}Fe_2O_4$ compositions. All observed reflections of the Co substituted Mn-Cu ferrite samples could be assigned to cubic spinel lattice indicating their single phase nature. Lattice constant (a) varies between 8.3379-8.3903 A^0. The crystallite size was in the range of 26–36 nm. It was observed that theoretical density increases with substitution of cobalt which confirms that, the addition of cobalt in manganese copper ferrites results in the increasing density of the material. The theoretical density of the ferrites was determined accurately by the hydrostatic method. Plot of theoretical density vs. cobalt content is shown in Fig. 2. It is also observed from the figure that theoretical density increases up to X=0.3 thereafter decreases for X=0.4 and further increase with Co content. Theoretical density, lattice constant (a), crystallite size (t) & X-ray density (d_x) are summarized in Table 1.

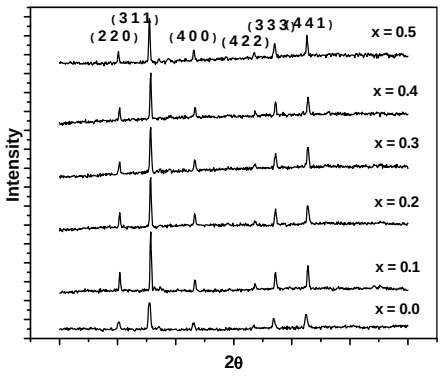

Fig. 1: X-ray Diffraction Patterns of the System $Mn_{0.5-X}Co_XCu_{0.5}Fe_2O_4$ ($0.0 \geq X \leq 0.5$)

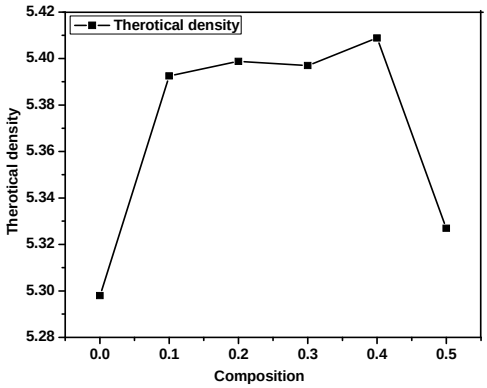

Fig. 2: Variation of theoretical density Vs Co content

3.2. Scanning Electron Microscopy

SEM micrographs of the samples are displayed in the Fig. 3(a–f). These figures indicate that samples obtained by this method are uniform in both morphology and crystallite size, but having agglomeration to some extent, due to the relative higher annealing temperature and interaction between magnetic particles. The agglomeration is due to the Van-der Waal forces between the particles [22]. Present study reveals that, all samples were of fine grains. The average grain size was calculated by Cottrell's method [23] and it remain in the range of 0.7 to 2.0μm. Average grain size of ferrite decreases from X=0.0 to X=0.5. Also it was observed that the porosity decreases with increasing grain size actual density (d_a), porosity (%P) and average grain size are summarized in which is summarized in Table 2.

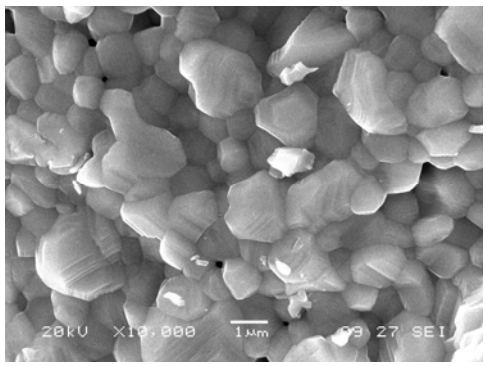

a (x=0.0)

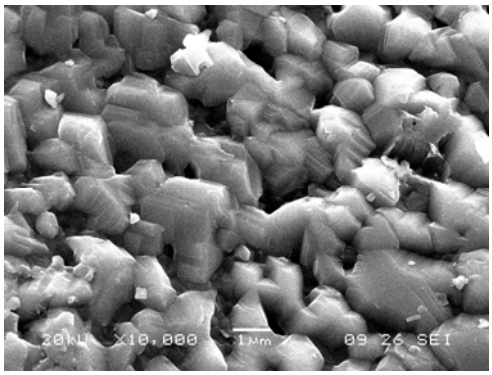

b (x=0.1)

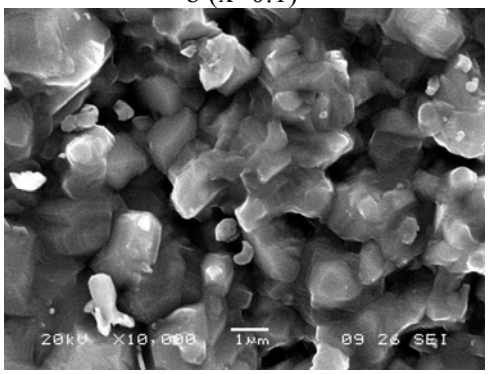

c (x=0.2)

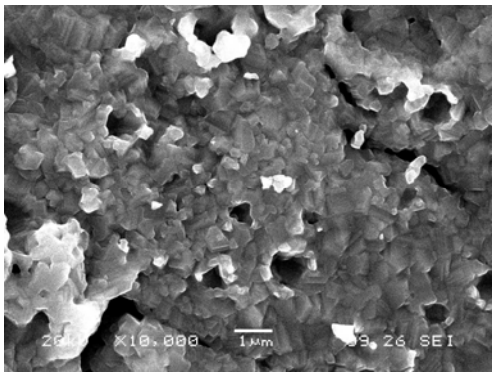

d (x=0.3)

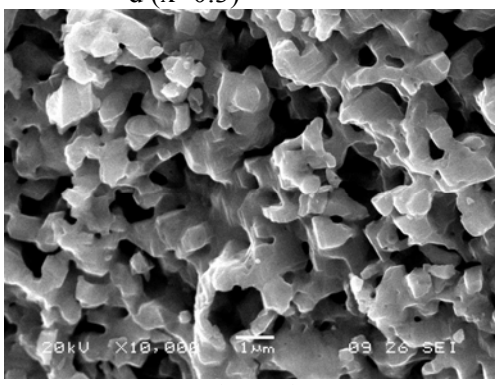

e (x=0.4)

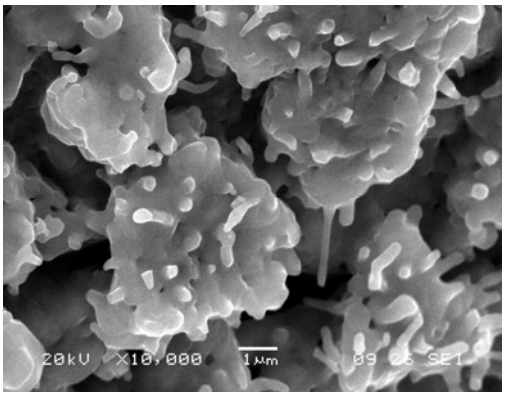

f (x=0.5)

Fig. 3 (a-f): SEM microstructures of $Mn_{0.5-x}Co_xCu_{0.5}Fe_2O_4$ ($0.0 \geq X \leq 0.5$)

Composition	Actual Density (d_a) gm/cm^3	Porosity (P) %	Average Grain Size (μm)
0.0	6.7600	21.6	2.1
0.1	6.3503	15.0	1.85
0.2	6.4267	15.9	1.6
0.3	6.5286	17.3	0.728
0.4	6.6942	19.2	0.721
0.5	6.0891	12.5	0.720

Table 2– Actual density (d_a), Porosity (%P) and Average grain size from SEM

3.3. Energy dispersive X-ray analysis

The composition of the metal oxides had been determined by using the energy dispersive X-ray analysis (EDAX) [24]. X-ray analysis spectrum of $Mn_{0.5-x}Co_xCu_{0.5}Fe_2O_4$ (X=0.0, 0.2, 0.5) is shown in Fig. 4(a-c). The presence of Mn, Co, Cu, Fe and O are confirmed in all samples from EDAX spectrum. Spectrum analysis proved the stoichiometries of $Mn_{0.5-x}Co_xCu_{0.5}Fe_2O_4$ (X=0.0, 0.2, 0.5) ferrites synthesized by sol gel auto combustion method. Analysis did not indicate the presence of any foreign elements in it. This confirms the purity and the composition of the material.

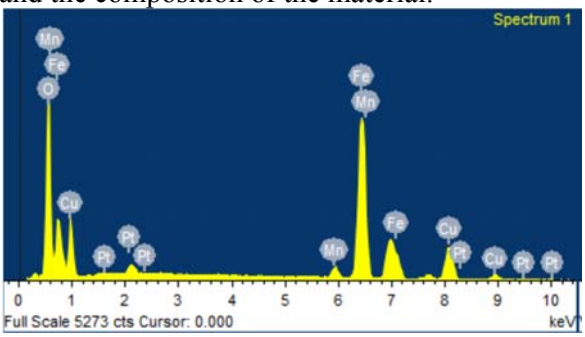

a (X=0.0)

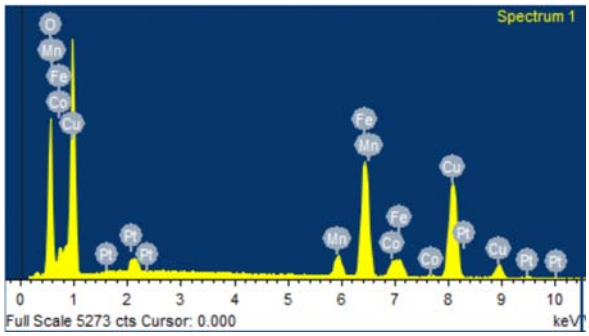

b (X=0.2)

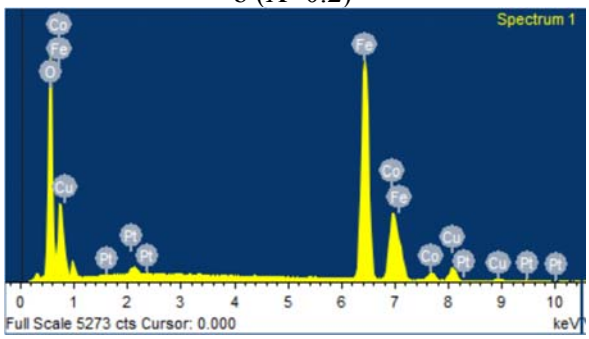

c (X=0.5)

Fig. 4: EDAX spectra of $Mn_{0.5-x}Co_xCu_{0.5}Fe_2O_4$ (X=0.0, 0.2, 0.5)

3.4. Thermal Analysis

TGA curve [Fig. 5(a-c)] shows that, at initial level there was 5 to 7% loss in weight because of removal of absorbed water and water of crystallization up to 200^0C. The observed weight loss is very minor which indicates the entire urea complex is decomposed during auto-combustion process. TGA curve doesn't indicate any variation in weight above 450^0C which highlights stability of cubic spinel structure.

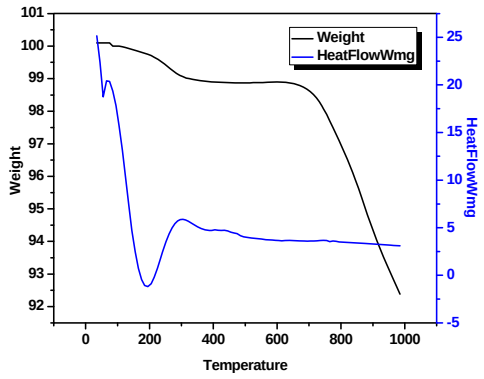

a (X=0.0)

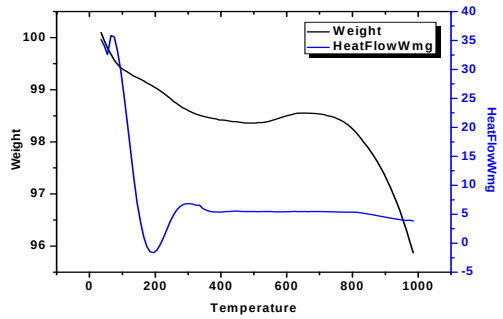

b (X=0.2)

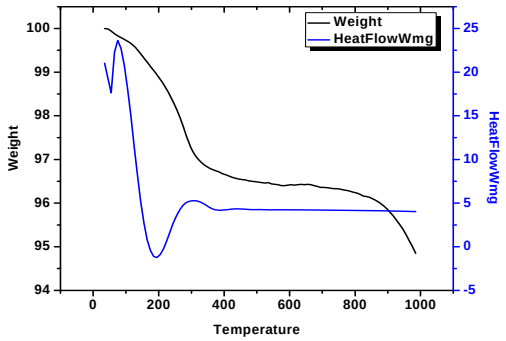

c (X=0.5)

Fig. 5: TG-DTA of $Mn_{0.5-x}Co_xCu_{0.5}Fe_2O_4$ (X=0.0, 0.2, 0.5)

3.5 DC Electrical Resistivity

Temperature dependent variation of dc resistivity for $Mn_{0.5-x}Co_xCu_{0.5}Fe_2O_4$ ($0.0 \geq X \leq 0.5$) is shown in Fig. 6. Linear decrease in resistivity with increasing temperature reflects semiconducting nature of material. The conduction mechanism in ferrites is explained on the basis of Verwey De Boer mechanism that involves exchange of electrons between the ions of the same elements present in more than one valence state and distributed randomly over equivalent crystallographic lattice sites. The decrease in resistivity with an increase in temperature is attributed to increases in drift mobility of the charge carriers. Also conduction in ferrites may be due to hopping of electrons from Fe^{3+} to Fe^{2+} ions. In transition metal oxides, it is observed that electrical resistivity is low when the compound contains the cation of the same element situated at the similar site but with their valency differing by unity [25]. Activation energy of all samples varies in range of 0.4692 0.6853eV.

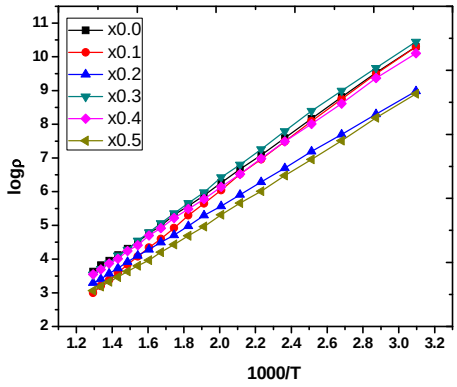

Fig. 6: DC Resistivity of $Mn_{0.5-x}Co_xCu_{0.5}Fe_2O_4$ ($0.0 \geq X \leq 0.5$)

3.6 Magnetic Properties

The substitution of Co ions, which has preferential A and B-site occupancies respectively, results in the reduction of the exchange interaction between -A and B-sites. Hence by varying the degree of Co substitution, the magnetic properties can be varied. Hysteresis loops at room temperature (300K) of $Mn_{0.5-x}Co_xCu_{0.5}Fe_2O_4$ ($0.0 \geq X \leq 0.5$) is shown in fig. 7. The values of saturation magnetization (M_s), coercivity (H_c) and magnetic moment (μ_B) measurements are listed in Table 3. Saturation magnetization of samples non-linearly varies from 27.313 to 41.823emu/g. Variation of Saturation Magnetization with Cobalt content is shown in Fig. 8. Also Co substitution results in increase of coercivity from 83.593 to 280.84 Oe.

In spinel ferrites magnetic properties depend on the sum of the magnetic moments at tetrahedral -A site and octahedral -B site [26]. The magnetic moment value in terms of Bohr magneton varies in the range of 1.1 to 1.7 with Co substitution. Saturation Magnetization first decreases with addition of Co then it increases non-linearly that is mostly due to Yafet and Kittel spin arrangement [27,28] and unequal distribution of Mn & Co on tetrahedral -A site and octahedral -B site of copper ferrites.

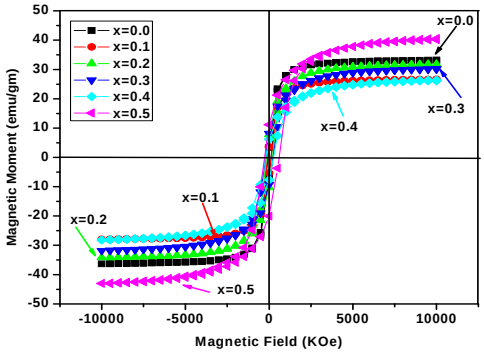

Fig. 7: Variation of magnetization with applied field for$Mn_{0.5-x}Co_xCu_{0.5}Fe_2O_4$ ($0.0 \geq X \leq 0.5$)

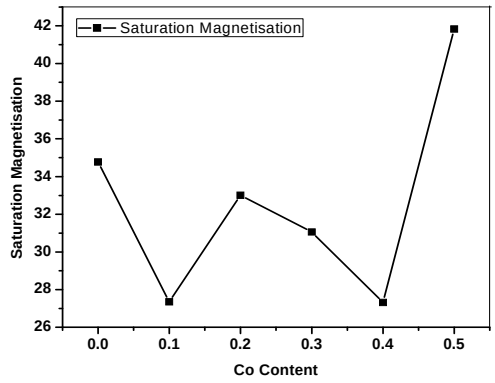

Fig. 8: Variation of Saturation Magnetization with Cobalt content.

Table 3- Data on magnetic hysteresis for $Mn_{0.5-x}Co_xCu_{0.5}Fe_2O_4$ system

Composition	Saturation Magnetization (M_s)emu/g	Coercivity H_c (Oe)	Magnetic Moment (μB) Bohr magneton
0.0	34.774	83.593	1.462
0.1	27.349	101.34	1.152
0.2	33.003	175.14	1.394
0.3	31.051	219.1	1.312
0.4	27.313	226.81	1.156
0.5	41.823	280.84	1.774

4. Conclusion

The pH controlled synthesis of $Mn_{0.5-x}Co_xCu_{0.5}Fe_2O_4$ ($0.0 \geq X \leq 0.5$) using a sol gel auto-combustion method is feasible. The crystal structures of ferrite samples (X=0.0 to X=0.5) were found cubic spinel. Experimental results revealed that, the lattice constant varies non-linearly and slight decrease in crystallite size

with the increase of Co content. Thermal analysis shows that ferrites are formed above 450^0C. Morphology studies shows that, average grain size decreases from 2.1 to 0.720 μm with addition of Co and elemental analysis of metals in the samples are in their stoichiometric proportions as expected. Electrical resistivity plot shows that nature of all samples is semiconducting. Activation energy varies in the range 0.4692 to 0.6853 eV. The magnetic moment value in terms of Bohr magneton varies in the range of 1.1 to 1.7 with Co substitution. The saturation magnetization changes non-linearly with Co content (27.313 to 41.823emu/g).

5. Acknowledgement

One of the authors (PDK) is thankful to SERB, New Delhi for sanctioning Major Research Project, SERB/F/5299/2016-17.

6. References:-

[1] Z. Jia, D. Ren, Y. Liang, R. Zhu, Mater. Lett. 65 (2011) 3116–3119.

[2] P.P. Hankare, P.D. Kamble, S.P. Maradur, M.R. Kadam, U.B. Sankpal, R.P. Patil, R.K. Nimat, P.D. Lokhande, J. Alloys Compd. 487 (2009) 730–734.

[3] J.K. Rajput, G. Kaur, Catal. Sci. Technol. 4 (2014) 142–151.

[4] G.A.E. Shobaky, A.M. Turky, N.Y. Mostafa, S.K. Mohamed, J. Alloys Compd. 493 (2010) 415–422.

[5] V. Pillai, D.O. Shah, J. Magn. Magn. Mater. 163 (1996) 243.

[6] S.Y. An, I.S. Kim, S.H. Son, S.Y. Song, J.W. Hahn, S.W. Hyun, C.M. Kim, C.S. Kim, Thin Solid Films 519 (2011) 8296–8298.

[7] I. Nedkov, R.E. Vandenberghe, Ts. Marinova, Ph. Thailhades, T. Merodiiska, I. Avramova, Applied Surface Science 253 (2006) 2589–2596.

[8] P.P. Hankare, P.D. Kamble, M.R. Kadam, K.S. Rane, P.N. Vasambekar, Materials Letters 61 (2007) 2769–2771.

[9] S. Gautam, S. Muthurani, M. Balaji, P. Thakur, Journal of Nanotechnology 11 (2011) 386.

[10] A.S. Albuquerque, J.D. Ardisson, W.A.A. Macedo, J.L. Lopez, R. Paniago, A.I.C. Persiano, J. Magn. Magn. Mater. 226 (2001) 1379.

[11] M. George, A.M. John, S.S. Nair, P.A. Joy, M.R. Anantharaman, J. Magn. Magn. Mater. 302 (2006) 190.

[12] P.S. Jadhav, K.K. Patankar, Vijaya Puri, Materials Research Bulletin 75 (2016) 162.

[13] S.S. Kumbhar, M.A. Mahadik, V.S. Mohite, Y.M. Hunge, K.Y. Rajpure, C.H. Bhosale, Materials Research Bulletin 67 (2015) 47

[14] S. Thompson, N.J. Shirtcliffe, E. O'keefe, S. Appleton, C.C. Perry, J. Magn. Magn. Mater. 292 (2005) 100.

[15] Yuksel Koseoglu, Ceramics International 39 (2013) 4221.

[16] J. Giri, T. Sriharsha, D. Bhadur, J. Mater. Chem. 14 (2004) 875.

[17] M.R. Kadam, R.P. Patil, P.P. Hankare, J. Solid State Sci. 14 (2012) 964-970.

[18] J.A. Rodriguez, M. Fernandez-Garcia, Textbook of Synthesis, Properties and Applications of Oxide Nanomaterials, Wiley Interscience, A John Wiley and Sons, Inc. Publication, 2007, p. 95.

[19] Hichem Huili, Bilel Grindia, Abdessalem Kouki, Guillaume Viau, Lotfi Ben Tahara, Ceramics International 41 (2015) 6212.

[20] P.P. Hankare, M.R. Kadam, R.P. Patil, K.M. Garadkar, R. Sasikala, A.K. Tripathi, Journal of Alloys and Compounds 501 (2010) 37.

[21] Jan Smit, Book of Magnetic Properties of Materials, Intra-University Electronics Series, 13, McGraw-Hill Book Co, New York, 1971, 89.

[22] K. Maaz, Arif Mumtaz, S. K. Hasanain, Abdullah Ceylan, Journal of Magnetism and Magnetic Materials 308 (2007) 289–295.

[23] A. Cottrell, An Introduction to Metallurgy, Edward Arnold, London, 1967.

[24] Satyendra Singh, B.C. Yadav, V.D. Gupta, Prabhat K. Dwivedi, Materials Research Bulletin, 47 (2012) 3538–3547.

[25] V. Edward, H. Bongio, F.C. Black, D. Raszewski, C. Edwards, J. Mcconville, V.R.W. Amarakoon, J. Electroceram. 14 (2005) 193.

[26] S.K. Pradhan, S. Bid, M. Gateshki, V. Petkov, Mater. Chem. Phys. 93 (2005) 224.

[27] Y. Yafet, C. Kittel, Phys. Rev. 90 (1952) 295.

[28] S.P. Yadav, S.S. Shinde, Pramod Bhatt, S.S. Meena, K.Y. Rajpure, Journal of Alloys and Compounds 646 (2015) 55